Erschienen in: Optics Letters ; 42 (2017), 10. - S. 2050-2053
https://dx.doi.org/10.1364/OL.42.002050

Ultrabroadband out-of-loop characterization of the carrier-envelope phase noise of an offset-free Er:fiber frequency comb

Andreas Liehl, David Fehrenbacher, Philipp Sulzer, Alfred Leitenstorfer, and Denis V. Seletskiy*

Department of Physics and Center for Applied Photonics, University of Konstanz, D-78457 Konstanz, Germany
**Corresponding author: denis.seletskiy@uni-konstanz.de*

Recent demonstrations of passively phase-locked fiber-based combs motivate broadband characterization of the noise associated with the stabilized carrier-envelope offset frequency. In our study, we analyze the phase noise of a 100 MHz Er:fiber system in a wide range spanning from microhertz to the Nyquist frequency. An interferometric detection method enables analysis of the high-frequency output of an f-to-2f interferometer. The dominant contribution of a broadband white noise floor at high frequencies attests quantum-limited performance. An out-of-loop measurement of the carrier-envelope phase reveals its jitter to be as low as 250 mrad when integrated over 12 orders of magnitude of the radio-frequency spectrum.

Next generations of precision atomic clocks [1,2] demand advanced ultralow-noise frequency dividers based on femtosecond frequency combs [3,4]. Such optical frequency rulers enable a variety of high-precision applications like optical frequency synthesis, frequency comb spectroscopy, and light detection and ranging (LIDAR) systems as well as ultrastable microwave generation [5–7]. Femtosecond frequency combs serving as optical clockworks require the stabilization of two fundamental degrees of freedom: the repetition rate f_{rep} and the carrier-envelope offset (CEO) frequency f_{CEO}. The repetition rate is directly accessible through the radio-frequency (RF) signal of the intensity of the pulse train. In contrast, the direct determination of the CEO frequency requires at least one nonlinear optical process [8] with the f-to-2f self-referencing technique being most widespread [9,10]. Once detected, f_{CEO} can be actively stabilized to an RF reference by employing electronic feedback to either the pump power of the oscillator [9] or fast intracavity modulators [10]. Since the first application of similar approaches to fiber-based frequency combs [11,12], lots of progress has been achieved to improve their overall phase noise performance [13–19]. Accumulation of excess phase jitter around the frequency cutoff of the feedback loop represents a shared drawback of active stabilization. A feed-forward scheme based on an extracavity acousto-optic element elegantly circumventing such limitations has been successfully implemented in solid-state oscillators [20] and amplifiers [21]. Difference frequency generation (DFG) within a broadband optical spectrum provides an entirely passive approach to eliminate the carrier-envelope phase (CEP) slip [22–24], thus setting f_{CEO} to zero with an effective locking bandwidth of the full repetition rate. Our recent implementation of this passive phase-locking technique in the context of an Er:fiber comb [25] demonstrated the root-mean-square (RMS) value of the remaining CEP fluctuations to be 219 mrad over 8 s. While such levels are already attractive for high-precision metrology, a close analysis of the pulse-to-pulse evolution of the CEP is indispensable for investigations of nonperturbative nonlinear phenomena at high repetition rates. In addition, analysis of the CEP noise over the full RF bandwidth of a pulse train provides insight into the origin of the optical linewidth of the comb [26].

Motivated by these considerations, we investigate the spectral density of the CEP noise of a passively phase-locked 100 MHz Er:fiber frequency comb up to the Nyquist frequency. High bandwidth of the measurement is enabled by a new detection scheme which extends the traditional f-to-2f interferometer measurements for characterization of slow drifts of the CEP [27]. We note that by virtue of passive phase-locking, our CEP noise analysis is inherently "out-of-loop" (OOL). Such measurements are crucial since external perturbations to the pulse train, for example during amplification or by extracavity optical elements, do not necessarily contribute to in-loop characterization schemes, but nonetheless, they can significantly influence the overall phase noise [28]. OOL measurements of the CEP noise up to the Nyquist frequency have been performed on mode-locked Ti:sapphire lasers, for instance, by using a 0-to-f monolithic interferometer [29]. We are aware of only a few OOL measurements of the CEP noise of mode-locked fiber lasers, all at a few megahertz bandwidth [16,30,31].

The experimental setup for the generation of an offset-free Er:fiber-based frequency comb [32] is shown in the top green box of Fig. 1. An all-fiber solitonic oscillator consisting of only

polarization-maintaining components emits a stable pulse train with a repetition rate of 100 MHz and a pulse energy of approximately 50 pJ. Mode-locking is achieved with a saturable absorber mirror. The central wavelength of the output is 1556 nm (193 THz). The pulse energy is boosted to 6 nJ by means of an erbium-doped fiber amplifier (EDFA), and the pulses are compressed to a duration of 115 fs. These parameters enable generation of an ultrabroad spectrum within a dispersion-managed highly nonlinear germanosilicate fiber (HNF). High spectral coherence of the output [33] enables the generation of an offset-free comb by DFG between regions of maximum power at opposite ends of the tailored supercontinuum which are separated by a frequency of 193 THz, where the following EDFA shows optimum performance [25]. We reamplify to the initial energy level of 6 nJ and compress the pulses to a duration of 105 fs. This process is divided into two steps: a preamplifier stage followed by the main amplifier. Although the preamplifier is not mandatory to obtain the final pulse energy, it offers two distinct advantages. First, it allows seeding of several parallel EDFAs well above their saturation threshold [34]. Second, the CEP of the pulses may be adjusted by controlling the pump power of the preamplifier. This feature is exploited for calibration of the CEP noise measurement.

The f-to-2f interferometer for determination of the CEP [27] is sketched in the blue box at the bottom of Fig. 1. Here, the pulse train is directed to a second HNF where we again generate a super-octave-spanning spectrum. Note that the CEO is preserved during the nonlinear frequency conversion since

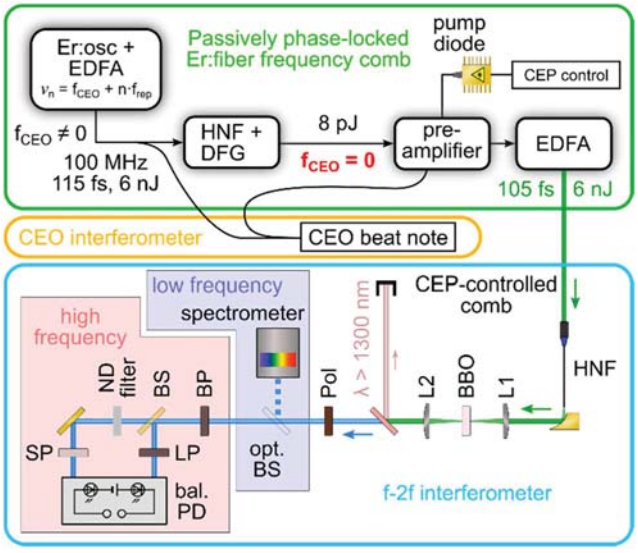

Fig. 1. Top: Sketch of the setup for the generation of a passively phase-locked Er:fiber frequency comb. The CEP can be precisely adjusted by the pump power of the preamplifier. Er:osc, Er:fiber-based oscillator; EDFA, erbium-doped fiber amplifier; HNF, highly nonlinear fiber; DFG, difference frequency generation unit. Center: CEO interferometer for generation of a CEO beat note by superimposing the fundamental and the phase-locked combs. Bottom: Sketch of the f-to-2f interferometer enabling CEP detection. Second HNF; L1, L2, lenses; BBO, β-barium borate crystal; Pol, polarizer; BS, beam splitters; BP, bandpass optical filter; ND filter, neutral density filter; SP, shortpass optical filter; LP, longpass optical filter; bal. PD, balanced differential photodetector.

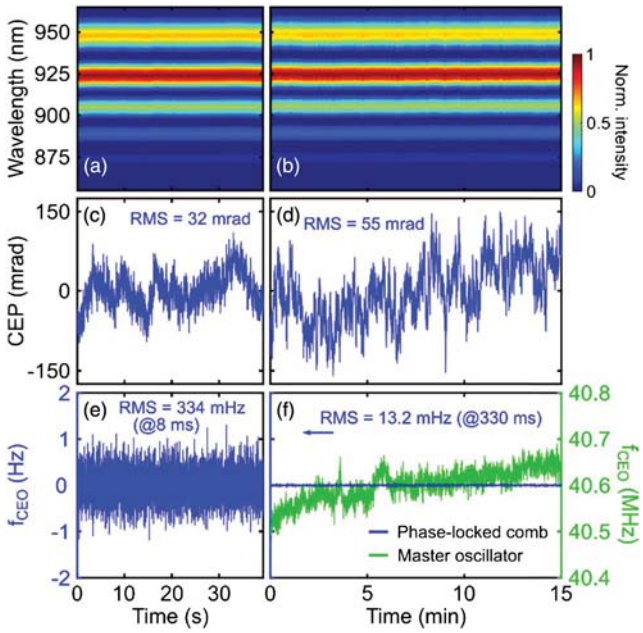

Fig. 2. (a) and (b) Time evolution of the spectral fringes at the output of the f-to-2f interferometer within an interval of 40 s and 15 min, respectively. (c) and (d) Time evolution of the CEP calculated from the interference spectra in (a) and (b), respectively. (e) and (f) CEO frequency of the phase-locked comb (blue) and the free-running master oscillator (green). The ordinate scale for blue graphs in panels (e) and (f) is on the left side of panel (e), while the ordinate for the green graph is depicted on the right of panel (f).

the spectral broadening is predominantly caused by four-wave-mixing processes [23]. The long-wavelength edge of the output spectrum of the HNF is frequency-doubled with a 2-mm-thick β-barium borate crystal (BBO) cut at an angle of 20° for type-I phase matching. A linear polarizer (Pol) is used to heterodyne the frequency-doubled radiation with the fundamental component at the same frequency. The evolution of the resulting interference fringes is recorded via a CCD-based spectrometer, enabling sensitive characterization of the CEP noise at low frequencies.

The temporal dynamics of the spectral interference pattern is shown in Fig. 2(a) for a 40 s time interval and an 8 ms single-frame acquisition time, while the period in Fig. 2(b) spans 15 min with 330 ms sample period. High fringe visibility (>99%) and no abrupt jumps are clearly observed on both short and long timescales. The CEP calculated from the interference spectra by a Fourier transform algorithm [27] is shown in Figs. 2(c) and 2(d). We observe phase fluctuations with RMS values as small as 32 and 55 mrad when sampled over 40 s and 15 min, respectively. Therefore, the average of f_{CEO} inherently vanishes and deviations remain in the millihertz range for those observation times [see blue graphs in Figs. 2(e) and 2(f)]. The relative stability of the CEO frequency at a wavelength of 920 nm and a gate time of 3 ms is 2×10^{-17}, which is superior as compared to previous reports on active CEO stabilization of fiber-based frequency combs when measured OOL [16,31]. During the measurement over 15 min, we simultaneously recorded the nonstabilized CEO frequency of the free-running master oscillator by detecting a CEO beat note between the oscillator output and the phase-locked comb (yellow box in

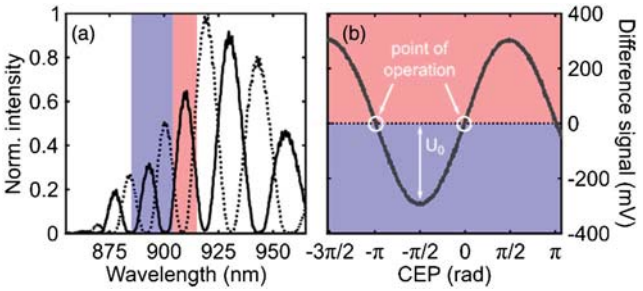

Fig. 3. (a) Comparison of interference pattern if $\varphi_{CEP} = \pi/2$ (solid) and $\varphi_{CEP} = -\pi/2$ (dotted). Red and blue shaded regions: bandwidth filtered within the two channels reaching the bal. PD. (b) Difference signal of the bal. PD as a function of CEP. Red and blue shaded regions: values of the difference signal where the spectral intensity is larger in the spectral range at longer and shorter wavelengths, respectively.

the center of Fig. 1). The time evolution of f_{CEO} of the oscillator is depicted by the green graph in Fig. 2(f). Note the vastly different scales for the CEO frequencies of the phase-locked comb and the oscillator. Within the entire 15 min period, the f_{CEO} of the latter drifts by approximately 200 kHz while the RMS value of the fluctuations of the locked CEO is only 13.2 mHz. This measurement shows that at this observation time, the drift of the CEO frequency caused by environmental perturbations is suppressed by more than seven orders of magnitude through the all-passive optical lock. To the best of our knowledge, this is the first direct comparison of the time evolution of the passively locked f_{CEO} and the nonstabilized CEO frequency, demonstrating the value of the passive CEO locking technique.

Although these results prove the CEP to be long-term stable, even at the minimum integration time of the CCD array a single interference readout averages over many thousands of pulses. Hence, a fast detection method is necessary if a characterization of the CEP noise up to the Nyquist frequency is desired. Therefore, we developed a new detection scheme which can address the high-frequency noise. The principle relies on tracking fast spectral shifts of an interference fringe by means of a balanced differential photodetector (bal. PD). To this end, a spectral band with a central wavelength of 900 nm and bandwidth of 25 nm is selected by a bandpass filter such that approximately two interference fringes remain. Afterwards, the beam is divided into two branches by a 50:50 nonpolarizing beam splitter (BS). They are directed to the input channels of the bal. PD. Each branch is transmitted through a long- (LP) and shortpass filter (SP), respectively, delivering the spectral bands depicted by red and blue shaded regions in Fig. 3(a) to one of the photodiodes, respectively. For the interference spectrum shown by the solid graph in Fig. 3(a), the spectrally integrated signal within the red channel is at its maximum while the signal in the blue channel is at its minimum. The situation is reversed when the CEP is shifted by π (dotted graph). In our scheme, the difference signal between the two channels ΔU can be calculated by

$$\Delta U = \int_{\omega_{cut}}^{\infty} \eta I(\omega) \mathrm{d}\omega - \int_{0}^{\omega_{cut}} \eta I(\omega) \mathrm{d}\omega = U_0 \sin \varphi_{CEP}, \quad \textbf{(1)}$$

where ω_{cut} is the cutoff frequency of the LP and SP filters, η is the detector efficiency (in general a frequency-dependent quantity), and U_0 is half of the peak-to-peak value of the difference signal when the CEP is swept over 2π. The sinusoidal behavior described in Eq. (1) is reproduced by the measurement in Fig. 3(b). Here, the red and blue shaded areas mark values of the difference signal where the photocurrent is larger in the branch with the LP and SP filters, respectively. In order to obtain an offset-free harmonic dependence [Eq. (1)], we included a variable neutral density (ND) filter in one branch. At a balance point where the CEP is set to zero or multiple integers of π [points of operation marked with white circles in Fig. 3(b)], the difference signal vanishes and the sine function can be linearized for small arguments, resulting in direct proportionality of ΔU and the CEP angle. By measuring the amplitude noise density $S_{\Delta U}(f)$ of the difference signal with an RF spectrum analyzer, we directly obtain the CEP noise density $S_{CEP}(f) = S_{\Delta U}(f)/U_0^2$.

Figure 4 shows the resulting S_{CEP} (red graph) as well as the calculated noise densities obtained from the low-frequency measurements with the CCD array (blue graphs). The low-frequency analysis is split into three datasets with different acquisition times in order to avoid excess data accumulation (graphs of different blue shades in Fig. 4). The good match between the low- and high-bandwidth techniques around 100 Hz attests high reliability of the calibration. Our overall characterization provides a panoramic view of the spectral noise density of the CEP over 12 orders of magnitude of the RF spectrum. We identify three distinct regions. For frequencies below 1 kHz, flicker noise builds up according to acoustic and mechanical vibrations as well as accumulation of slow drifts. Around 10 kHz, a small but noticeable broadband feature can be attributed to the amplitude noise of the oscillator, which exhibits low-pass characteristics with a roll-off at 13 kHz (not shown) as a consequence of the upper-state lifetime of the Er^{3+} ions in the lasing cavity [35]. Through the nonlinearities of the optical fibers, amplitude-to-phase conversion can impact the CEP jitter. At 100 kHz, the CEP noise density reaches a white noise floor. With an average power of 50 μW impinging on

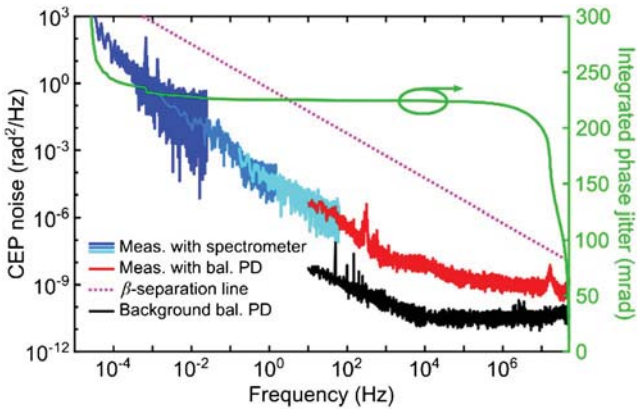

Fig. 4. CEP noise from the Nyquist frequency of 50 MHz down to 50 μHz measured by the spectrometer with three different acquisition times (blue) and the balanced photodetector (red). The dark noise of the bal. PD is shown in black. The entire phase noise spectrum resides far below the β-separation line (pink dotted line), indicating a negligible influence on the optical comb linewidth. The green graph and right ordinate scale show the integrated phase jitter.

each channel of the bal. PD, the estimated shot noise contribution amounts to 10^{-14} rad^2/Hz. Hence, the observed feature cannot result from the detection shot noise. This is further verified since no change of the noise level is observed when the peak power is attenuated immediately before the bal. PD. This finding suggests a quantum origin of the CEP noise [36], which is consistent with the quantum-limited performance of our soliton-based passively phase-locked frequency comb [32]. We emphasize that no sharp features are observed in the noise spectra, which are typically ascribed to limitations in the servo bandwidth for actively stabilized combs. Furthermore, the CEP noise density stays well below the β-separation line over the entire analyzed frequency range (pink dotted graph in Fig. 4). This fact proves that CEP noise does not significantly contribute to the optical linewidth of the comb [26], which remains dominated by fluctuations of the repetition rate [32]. An integrated phase jitter of 250 mrad is obtained when integrating from the Nyquist frequency of 50 MHz down to 50 μHz (green graph in Fig. 4). This value corresponds to an integrated timing jitter of 200 as at the central wavelength of the frequency comb of 1556 nm. This result compares favorably with the record performance demonstrated for actively stabilized combs based on solid-state lasers [37] when integrating over a comparable RF range. Only if investigated over several days do thermal drifts cause the phase jitter to exceed one optical cycle. However, such effects could be easily removed by an active temperature stabilization or a feedback loop to the pump power of the preamplifier operating with subhertz bandwidth.

In conclusion, we have measured the OOL CEP noise of a passively phase-locked 100 MHz Er:fiber frequency comb over 12 orders of magnitude in RF, enabled by the novel broadband detection scheme. The integrated RMS of the CEP is at a record-low 250 mrad and predominantly of quantum origin. The resulting sub-200-as timing jitter demonstrates passively phase-locked Er:fiber frequency combs as superb sources not only for precision metrology but also for time-domain applications operating at the Nyquist sampling limit. Finally, the multi-megahertz detection capability of f_{CEO} that we demonstrated might also be beneficial in situations where extremely broadband feedback is required for stabilization.

Funding. H2020 European Research Council (ERC) (290876).

REFERENCES

1. M. Takamoto, F.-L. Hong, R. Higashi, and H. Katori, Nature **435**, 321 (2005).
2. T. L. Nicholson, S. L. Campbell, R. B. Hutson, G. E. Marti, B. J. Bloom, R. L. McNally, W. Zhang, M. D. Barrett, M. S. Safronova, G. F. Strouse, W. L. Tew, and J. Ye, Nat. Commun. **6**, 6896 (2015).
3. J. L. Hall, Rev. Mod. Phys. **78**, 1279 (2006).
4. T. W. Hänsch, Rev. Mod. Phys. **78**, 1297 (2006).
5. S. T. Cundiff and J. Ye, Rev. Mod. Phys. **75**, 325 (2003).
6. S. A. Diddams, J. Opt. Soc. Am. B **27**, B51 (2010).
7. N. R. Newbury, Nat. Photonics **5**, 186 (2011).
8. H. R. Telle, G. Steinmeyer, A. E. Dunlop, J. Stenger, D. H. Sutter, and U. Keller, Appl. Phys. B **69**, 327 (1999).
9. R. Holzwarth, T. Udem, T. W. Hänsch, J. C. Knight, W. J. Wadsworth, and P. St. J. Russell, Phys. Rev. Lett. **85**, 2264 (2000).
10. D. J. Jones, S. A. Diddams, J. K. Ranka, A. Stentz, R. S. Windeler, J. L. Hall, and S. T. Cundiff, Science **288**, 635 (2000).
11. F. Tauser, A. Leitenstorfer, and W. Zinth, Opt. Express **11**, 594 (2003).
12. B. R. Washburn, S. A. Diddams, N. R. Newbury, J. W. Nicholson, M. F. Yan, and C. G. Jørgensen, Opt. Lett. **29**, 250 (2004).
13. D. D. Hudson, K. W. Holman, R. J. Jones, S. T. Cundiff, and D. J. Jones, Opt. Lett. **30**, 2948 (2005).
14. J. J. McFerran, W. C. Swann, B. R. Washburn, and N. R. Newbury, Appl. Phys. B **86**, 219 (2006).
15. L. Nugent-Glandorf, T. A. Johnson, Y. Kobayashi, and S. A. Diddams, Opt. Lett. **36**, 1578 (2011).
16. K. Iwakuni, H. Inaba, Y. Nakajima, T. Kobayashi, K. Hosaka, A. Onae, and F.-L. Hong, Opt. Express **20**, 13769 (2012).
17. L. C. Sinclair, J.-D. Deschênes, L. Sonderhouse, W. C. Swann, I. H. Khader, E. Baumann, N. R. Newbury, and I. Coddington, Rev. Sci. Instrum. **86**, 081301 (2015).
18. N. Kuse, C.-C. Lee, J. Jiang, C. Mohr, T. R. Schibli, and M. E. Fermann, Opt. Express **23**, 24342 (2015).
19. T. Puppe, A. Sell, R. Kliese, N. Hoghooghi, A. Zack, and W. Kaenders, Opt. Lett. **41**, 1877 (2016).
20. S. Koke, C. Grebing, H. Frei, A. Anderson, A. Assion, and G. Steinmeyer, Nat. Photonics **4**, 462 (2010).
21. T. Balčiūnas, T. Flöry, A. Baltuška, T. Stanislauskas, R. Antipenkov, A. Varanavičius, and G. Steinmeyer, Opt. Lett. **39**, 1669 (2014).
22. R. Huber, A. Brodschelm, F. Tauser, and A. Leitenstorfer, Appl. Phys. Lett. **76**, 3191 (2000).
23. A. Baltuška, T. Fuji, and T. Kobayashi, Phys. Rev. Lett. **88**, 133901 (2002).
24. M. Zimmermann, C. Gohle, R. Holzwarth, T. Udem, and T. W. Hänsch, Opt. Lett. **29**, 310 (2004).
25. G. Krauss, D. Fehrenbacher, D. Brida, C. Riek, A. Sell, R. Huber, and A. Leitenstorfer, Opt. Lett. **36**, 540 (2011).
26. G. Di Domenico, S. Schilt, and P. Thomann, Appl. Opt. **49**, 4801 (2010).
27. M. Kakehata, H. Takada, Y. Kobayashi, Y. Fujihara, K. Torizuka, Y. Fujihara, T. Homma, and H. Takahashi, Opt. Lett. **26**, 1436 (2001).
28. T. M. Fortier, D. J. Jones, J. Ye, S. T. Cundiff, and R. S. Windeler, Opt. Lett. **27**, 1436 (2002).
29. T. Fuji, J. Rauschenberger, C. Gohle, A. Apolonski, T. Udem, V. S. Yakovlev, G. Tempea, T. W. Hänsch, and F. Krausz, New J. Phys. **7**, 116 (2005).
30. G. Ycas, S. Osterman, and S. A. Diddams, Opt. Lett. **37**, 2199 (2012).
31. M. Giunta, W. Hänsel, K. Beha, M. Fischer, M. Lezius, and R. Holzwarth, *Conference on Lasers and Electro-Optics*, OSA Technical Digest (Optical Society of America, 2016), paper STh4H.1.
32. D. Fehrenbacher, P. Sulzer, A. Liehl, T. Kälberer, C. Riek, D. V. Seletskiy, and A. Leitenstorfer, Optica **2**, 917 (2015).
33. S. Kumkar, G. Krauss, M. Wunram, D. Fehrenbacher, U. Demirbas, D. Brida, and A. Leitenstorfer, Opt. Lett. **37**, 554 (2012).
34. F. Adler, A. Sell, F. Sotier, R. Huber, and A. Leitenstorfer, Opt. Lett. **32**, 3504 (2007).
35. B. R. Washburn, W. C. Swann, and N. R. Newbury, Opt. Express **13**, 10622 (2005).
36. N. R. Newbury and W. C. Swann, J. Opt. Soc. Am. B **24**, 1756 (2007).
37. B. Borchers, S. Koke, A. Husakou, J. Herrmann, and G. Steinmeyer, Opt. Lett. **36**, 4146 (2011).